

1 **MitoChime: A Machine-Learning Pipeline for**
2 **Detecting PCR-Induced Chimeras in**
3 **Mitochondrial Illumina Reads**

4 A Special Project Proposal
5 Presented to
6 the Faculty of the Division of Physical Sciences and Mathematics
7 College of Arts and Sciences
8 University of the Philippines Visayas
9 Miag-ao, Iloilo

10 In Partial Fulfillment
11 of the Requirements for the Degree of
12 Bachelor of Science in Computer Science

13 by

14 Duranne Duran
15 Yvonne Lin
16 Daniella Pailden

17 Adviser
18 Francis D. Dimzon, Ph.D.

19 December 5, 2025

Contents

21	1 Introduction	1
22	1.1 Overview	1
23	1.2 Problem Statement	3
24	1.3 Research Objectives	4
25	1.3.1 General Objective	4
26	1.3.2 Specific Objectives	4
27	1.4 Scope and Limitations of the Research	5
28	1.5 Significance of the Research	6
29	2 Review of Related Literature	7
30	2.1 The Mitochondrial Genome	7
31	2.1.1 Mitochondrial Genome Assembly	8

32	2.2 PCR Amplification and Chimera Formation	9
33	2.3 Existing Traditional Approaches for Chimera Detection	10
34	2.3.1 UCHIME	11
35	2.3.2 UCHIME2	12
36	2.3.3 CATch	13
37	2.3.4 ChimPipe	14
38	2.4 Machine Learning Approaches for Chimera and Sequence Quality	
39	Detection	15
40	2.4.1 Feature-Based Representations of Genomic Sequences . . .	15
41	2.5 Synthesis of Chimera Detection Approaches	16
42	3 Research Methodology	19
43	3.1 Research Activities	19
44	3.1.1 Data Collection	20
45	3.1.2 Feature Extraction Pipeline	24
46	3.1.3 Machine Learning Model Development	27
47	3.1.4 Model Benchmarking, Hyperparameter Optimization, and	
48	Evaluation	28
49	3.1.5 Feature Importance and Interpretation	29

50	3.1.6 Validation and Testing	30
51	3.1.7 Documentation	31
52	3.2 Calendar of Activities	32
53	4 Results and Discussion	33
54	4.1 Descriptive Analysis of Features	33
55	4.1.1 Univariate Distributions	34
56	4.2 Baseline Classification Performance	36
57	4.3 Effect of Hyperparameter Tuning	37
58	4.4 Detailed Evaluation of Representative Models	39
59	4.4.1 Confusion Matrices and Error Patterns	40
60	4.4.2 ROC and Precision–Recall Curves	41
61	4.5 Feature Importance and Biological Interpretation	43
62	4.5.1 Permutation Importance of Individual Features	43
63	4.5.2 Feature Family Importance	44
64	4.6 Summary of Findings	46

⁶⁵ List of Figures

⁶⁶	3.1 Process Diagram of Special Project	20
⁶⁷	4.1 Kernel density plots of six key features comparing clean and	
⁶⁸	chimeric reads.	35
⁶⁹	4.2 Test F1 of all baseline classifiers, showing that no single model	
⁷⁰	clearly dominates and several achieve comparable performance. . .	37
⁷¹	4.3 Comparison of test F1 (left) and ROC–AUC (right) for baseline and	
⁷²	tuned models. Hyperparameter tuning yields small but consistent	
⁷³	gains, particularly for tree-based ensembles.	39
⁷⁴	4.4 Confusion matrices for the four representative models on the held-	
⁷⁵	out test set. All models show more false negatives (chimeric reads	
⁷⁶	called clean) than false positives.	41
⁷⁷	4.5 ROC (left) and precision–recall (right) curves for the four represen-	
⁷⁸	tative models on the held-out test set. Tree-based ensembles cluster	
⁷⁹	closely, with logistic regression performing slightly but consistently	
⁸⁰	worse.	42

81	4.6 Permutation-based feature importance for four representative clas-	
82	sifiers. Clipping and k-mer composition features are generally the	
83	strongest predictors, whereas microhomology and other alignment	
84	metrics contribute minimally.	44
85	4.7 Aggregated feature family importance across four models. Clipping	
86	and k-mer compositional shifts are consistently the dominant con-	
87	tributors, while SA_structure, Micro_homology, and other features	
88	contribute minimally.	46

⁸⁹ List of Tables

⁹⁴ **Chapter 1**

⁹⁵ **Introduction**

⁹⁶ **1.1 Overview**

⁹⁷ The rapid advancement of next-generation sequencing (NGS) technologies has
⁹⁸ transformed genomic research by enabling high-throughput and cost-effective
⁹⁹ DNA analysis (Metzker, 2010). Among current platforms, Illumina sequencing
¹⁰⁰ remains the most widely adopted, capable of producing millions of short reads
¹⁰¹ that can be assembled into reference genomes or analyzed for genetic variation
¹⁰² (Bentley et al., 2008; Glenn, 2011). Despite its high base-calling accuracy,
¹⁰³ Illumina sequencing is prone to artifacts introduced during library preparation,
¹⁰⁴ particularly polymerase chain reaction (PCR)-induced chimeras, which are ar-
¹⁰⁵ tificial hybrid sequences that do not exist in the true genome (Judo, Wedel, &
¹⁰⁶ Wilson, 1998).

¹⁰⁷ PCR chimeras form when incomplete extension products from one template

anneal to an unrelated DNA fragment and are extended, creating recombinant reads (Qiu et al., 2001). In mitochondrial genome assembly, such artifacts are especially problematic because the mitochondrial genome is small, circular, and often repetitive (Boore, 1999; Cameron, 2014). Even a small number of chimeric or misjoined reads can reduce assembly contiguity and introduce false junctions during organelle genome reconstruction (Dierckxsens, Mardulyn, & Smits, 2017; Hahn, Bachmann, & Chevreux, 2013; Jin et al., 2020). Existing assembly tools such as GetOrganelle and MITObim assume that input reads are largely free of such artifacts (Hahn et al., 2013; Jin et al., 2020). Consequently, undetected chimeras may produce fragmented assemblies or misidentified organellar boundaries. To ensure accurate reconstruction of mitochondrial genomes, a reliable method for detecting and filtering PCR-induced chimeras before assembly is essential.

This study focuses on mitochondrial sequencing data from the genus *Sardinella*, a group of small pelagic fishes widely distributed in Philippine waters. Among them, *Sardinella lemuru* (Bali sardinella) is one of the country's most abundant and economically important species, providing protein and livelihood to coastal communities (Labrador, Agmata, Palermo, Ravago-Gotanco, & Pante, 2021; Willette, Bognot, Mutia, & Santos, 2011). Accurate mitochondrial assemblies are critical for understanding its population genetics, stock structure, and evolutionary history. However, assembly pipelines often encounter errors or fail to complete due to undetected chimeric reads. To address this gap, this research introduces MitoChime, a machine learning pipeline designed to detect and filter PCR-induced chimeric reads using both alignment-based and sequence-derived statistical features. The tool aims to provide bioinformatics laboratories, partic-

₁₃₃ ularly the Philippine Genome Center Visayas (PGC Visayas), with an efficient
₁₃₄ solution for improving mitochondrial genome reconstruction.

₁₃₅ 1.2 Problem Statement

₁₃₆ While NGS technologies have revolutionized genomic data acquisition, the ac-
₁₃₇ curacy of mitochondrial genome assembly remains limited by artifacts produced
₁₃₈ during PCR amplification. These chimeric reads can distort assembly graphs and
₁₃₉ cause misassemblies, with particularly severe effects in small, circular mitochon-
₁₄₀ drial genomes (Boore, 1999; Cameron, 2014). Existing assembly pipelines such
₁₄₁ as GetOrganelle, MITObim, and NOVOPlasty assume that sequencing reads are
₁₄₂ free of such artifacts (Dierckxsens et al., 2017; Hahn et al., 2013; Jin et al., 2020).
₁₄₃ At PGC Visayas, several mitochondrial assemblies have failed or yielded incom-
₁₄₄ plete contigs despite sufficient coverage, suggesting that undetected chimeric reads
₁₄₅ compromise assembly reliability. Meanwhile, existing chimera detection tools such
₁₄₆ as UCHIME and VSEARCH were developed primarily for amplicon-based com-
₁₄₇ munity analysis and rely heavily on reference or taxonomic comparisons (Edgar,
₁₄₈ Haas, Clemente, Quince, & Knight, 2011; Rognes, Flouri, Nichols, Quince, &
₁₄₉ Mahé, 2016). These approaches are unsuitable for single-species organellar data,
₁₅₀ where complete reference genomes are often unavailable. Therefore, there is a
₁₅₁ pressing need for a reference-independent, data-driven tool capable of detecting
₁₅₂ and filtering PCR-induced chimeras in mitochondrial sequencing datasets.

₁₅₃ **1.3 Research Objectives**

₁₅₄ **1.3.1 General Objective**

₁₅₅ This study aims to develop and evaluate a machine learning-based pipeline (Mi-
₁₅₆ toChime) that detects PCR-induced chimeric reads in *Sardinella lemuru* mito-
₁₅₇ chondrial sequencing data in order to improve the quality and reliability of down-
₁₅₈ stream mitochondrial genome assemblies.

₁₅₉ **1.3.2 Specific Objectives**

₁₆₀ Specifically, the study aims to:

- ₁₆₁ 1. construct simulated *Sardinella lemuru* Illumina paired-end datasets contain-
₁₆₂ ing both clean and PCR-induced chimeric reads,
- ₁₆₃ 2. extract alignment-based and sequence-based features such as k-mer compo-
₁₆₄ sition, junction complexity, and split-alignment counts from both clean and
₁₆₅ chimeric reads,
- ₁₆₆ 3. train, validate, and compare supervised machine-learning models for classi-
₁₆₇ fying reads as clean or chimeric,
- ₁₆₈ 4. determine feature importance and identify indicators of PCR-induced
₁₆₉ chimerism,
- ₁₇₀ 5. integrate the optimized classifier into a modular and interpretable pipeline
₁₇₁ deployable on standard computing environments at PGC Visayas.

172 1.4 Scope and Limitations of the Research

173 This study focuses on detecting PCR-induced chimeric reads in Illumina paired-
174 end mitochondrial sequencing data from *Sardinella lemuru*. The decision to re-
175 strict the taxonomic scope to a single species is based on four considerations: to
176 limit interspecific variation in mitochondrial genome size, GC content, and repeti-
177 tive regions so that differences in read patterns can be attributed more directly to
178 PCR-induced chimerism; to align the analysis with relevant *S. lemuru* sequencing
179 projects at PGC Visayas; to take advantage of the availability of *S. lemuru* mito-
180 chondrial assemblies and raw datasets in public repositories such as the National
181 Center for Biotechnology Information (NCBI), which facilitates reference selection
182 and benchmarking; and to develop a tool that directly supports local studies on
183 *S. lemuru* population structure and fisheries management.

184 The study emphasizes `wgsim`-based simulations and selected empirical mito-
185 chondrial datasets from *S. lemuru*. It excludes naturally occurring chimeras, nu-
186 clear mitochondrial pseudogenes (NUMTs), and large-scale assembly rearrange-
187 ments in nuclear genomes. Feature extraction is restricted to low-dimensional
188 alignment and sequence statistics, such as k-mer frequency profiles, GC content,
189 read length, soft and hard clipping metrics, split-alignment counts, and map-
190 ping quality, rather than high-dimensional deep learning embeddings. This de-
191 sign keeps model behaviour interpretable and ensures that the pipeline can be
192 run on standard workstations at PGC Visayas. Testing on long-read platforms
193 (e.g., Nanopore, PacBio) and other taxa is outside the scope of this project; the
194 implemented pipeline is evaluated only on short-read *S. lemuru* datasets.

195 Other limitations in this study include the following: simulations with varying

196 error rates were not performed, so the effect of different sequencing errors on model
197 performance remains unexplored; alternative parameter settings, including k-mer
198 lengths and microhomology window sizes, were not systematically tested, which
199 could affect the sensitivity of both k-mer and microhomology feature detection as
200 well as the identification of chimeric junctions; and the machine-learning models
201 rely on supervised training with labeled examples, which may limit their ability
202 to detect novel or unexpected chimeric patterns.

203 1.5 Significance of the Research

204 This research provides both methodological and practical contributions to mito-
205 chondrial genomics and bioinformatics. First, MitoChime detects PCR-induced
206 chimeric reads prior to genome assembly, with the goal of improving the con-
207 tiguity and correctness of *Sardinella lemuru* mitochondrial assemblies. Second,
208 it replaces informal manual curation with a documented workflow, improving au-
209 tomation and reproducibility. Third, the pipeline is designed to run on computing
210 infrastructures commonly available in regional laboratories, enabling routine use
211 at facilities such as PGC Visayas. Finally, more reliable mitochondrial assemblies
212 for *S. lemuru* provide a stronger basis for downstream applications in the field of
213 fisheries and genomics.

²¹⁴ **Chapter 2**

²¹⁵ **Review of Related Literature**

²¹⁶ This chapter presents an overview of the literature relevant to the study. It
²¹⁷ discusses the biological and computational foundations underlying mitochondrial
²¹⁸ genome analysis and assembly, as well as existing tools, algorithms, and techniques
²¹⁹ related to chimera detection and genome quality assessment. The chapter aims to
²²⁰ highlight the strengths, limitations, and research gaps in current approaches that
²²¹ motivate the development of the present study.

²²² **2.1 The Mitochondrial Genome**

²²³ Mitochondrial genome (mtDNA) is a small, typically circular molecule found in
²²⁴ most eukaryotes. It encodes essential genes involved in oxidative phosphorylation
²²⁵ and energy metabolism. Because of its conserved structure, mtDNA has become
²²⁶ a valuable genetic marker for studies in population genetics and phylogenetics
²²⁷ (Anderson et al., 1981; Boore, 1999). In animal species, the mitochondrial genome

ranges from 15–20 kilobase and contains 13 protein-coding genes, 22 tRNAs, and two rRNAs arranged compactly without introns (Gray, 2012). In comparison to nuclear DNA, the ratio of the number of copies of mtDNA is higher and has simple organization which make it particularly suitable for genome sequencing and assembly studies (Dierckxsens et al., 2017).

2.1.1 Mitochondrial Genome Assembly

Mitochondrial genome assembly refers to the reconstruction of the complete mitochondrial DNA (mtDNA) sequence from raw or fragmented sequencing reads. It is conducted to obtain high-quality, continuous representations of the mitochondrial genome that can be used for a wide range of analyses, including species identification, phylogenetic reconstruction, evolutionary studies, and investigations of mitochondrial diseases. Because mtDNA evolves rapidly, its assembled sequence provides valuable insights into population structure, lineage divergence, and adaptive evolution across taxa (Boore, 1999). Compared to nuclear genome assembly, assembling the mitochondrial genome is often considered more straightforward but still encounters technical challenges such as the formation of chimeric reads. Commonly used tools for mitogenome assembly such as GetOrganelle and MITObim operate under the assumption of organelle genome circularity, and are vulnerable when chimeric reads disrupt this circular structure, resulting in assembly errors (Hahn et al., 2013; Jin et al., 2020).

248 2.2 PCR Amplification and Chimera Formation

249 PCR plays an important role in NGS library preparation, as it amplifies target
250 DNA fragments for downstream analysis. However as previously mentioned, the
251 amplification process can also introduce chimeric reads which compromises the
252 quality of the input reads supplied to sequencing or assembly workflows. Chimeras
253 typically arise when incomplete extension occurs during a PCR cycle. This causes
254 the DNA polymerase to switch from one template to another and generate hy-
255 brid recombinant molecules (Judo et al., 1998). Artificial chimeras are produced
256 through such amplification errors, whereas biological chimeras occur naturally
257 through genomic rearrangements or transcriptional events.

258 In the context of amplicon-based sequencing, the presence of chimeras can in-
259 flate estimates of genetic or microbial diversity and may cause misassemblies dur-
260 ing genome reconstruction. Qin et al. (2023) has reported that chimeric sequences
261 may account for more than 10% of raw reads in amplicon datasets. This artifact
262 tends to be most prominent among rare operational taxonomic units (OTUs) or
263 singletons, which are sometimes misinterpreted as novel diversity, further caus-
264 ing the complication of microbial diversity analyses (Gonzalez, Zimmermann, &
265 Saiz-Jimenez, 2004). As such, determining and minimizing PCR-induced chimera
266 formation is vital for improving the quality of mitochondrial genome assemblies,
267 and ensuring the reliability of amplicon sequencing data.

268 **2.3 Existing Traditional Approaches for Chimera**

269 **Detection**

270 Several computational tools have been developed to identify chimeric sequences in
271 NGS datasets. These tools generally fall into two categories: reference-based and
272 de novo approaches. Reference-based chimera detection, also known as database-
273 dependent detection, is one of the earliest and most widely used computational
274 strategies for identifying chimeric sequences in amplicon-based community studies.
275 These methods rely on the comparison of each query sequence against a curated,
276 high-quality database of known, non-chimeric reference sequences (Edgar et al.,
277 2011).

278 On the other hand, the de novo chimera detection, also referred to as reference-
279 free detection, represents an alternative computational paradigm that identifies
280 chimeric sequences without reliance on external reference databases. This method
281 infer chimeras based on internal relationships among the sequences present within
282 the dataset itself, making it particularly advantageous in studies of under explored
283 or taxonomically diverse communities where comprehensive reference databases
284 are unavailable or incomplete (Edgar, 2016; Edgar et al., 2011). The underlying
285 assumption on this method is that during PCR, true biological sequences are
286 generally more abundant as they are amplified early and dominate the read pool,
287 whereas chimeric sequences appear later and are generally less abundant. The
288 de novo approach leverage this abundance hierarchy, treating the most abundant
289 sequences as supposed parents and testing whether less abundant sequences can
290 be reconstructed as mosaics of these templates. Compositional and structural
291 similarity are also evaluated to check whether different regions of a candidate

292 sequence correspond to distinct high-abundance sequences.

293 In practice, many modern bioinformatics pipelines combine both paradigms
294 sequentially: an initial de novo step identifies dataset-specific chimeras, followed
295 by a reference-based pass that removes remaining artifacts relative to established
296 databases (Edgar, 2016). These two methods of detection form the foundation of
297 tools such as UCHIME and later UCHIME2.

298 2.3.1 UCHIME

299 UCHIME is one of the most widely used tools for detecting chimeric sequences in
300 amplicon-based studies and remains a standard quality-control step in microbial
301 community analysis. Its core strategy is to test whether a query sequence (Q) can
302 be explained as a mosaic of two parent sequences, (A and B), and to score this
303 relationship using a structured alignment model (Edgar et al., 2011).

304 In reference mode, UCHIME divides the query into several segments and maps
305 them against a curated database of non-chimeric sequences. Candidate parents
306 are identified, and a three-way alignment is constructed. The algorithm assigns
307 “Yes” votes when different segments of the query match different parents and
308 “No” votes when the alignment contradicts a chimeric pattern. The final score
309 reflects the balance of these votes. In de novo mode, UCHIME operationalizes the
310 abundance-skew principle described earlier: high-abundance sequences are treated
311 as candidate parents, and lower-abundance sequences are evaluated as potential
312 mosaics. This makes the method especially useful when no reliable reference
313 database exists.

314 Although UCHIME is highly sensitive, it faces key constraints. Chimeras
315 formed from parents with very low divergence (below 0.8%) are difficult to de-
316 tect because they are nearly indistinguishable from sequencing errors. Accuracy
317 in reference mode depends strongly on database completeness, while de novo de-
318 tection assumes that true parents are both present and sufficiently more abun-
319 dant—conditions not always met in complex or unevenly amplified datasets.

320 **2.3.2 UCHIME2**

321 UCHIME2 extends the original algorithm with refinements tailored for high-
322 resolution sequencing data. One of its major contributions is a re-evaluation
323 of benchmarking practices. Edgar (2016) demonstrated that earlier accuracy es-
324 timates for chimera detection were overly optimistic because they relied on un-
325 realistic scenarios where all true parent sequences were assumed to be present.
326 Using the more rigorous CHSIMA benchmark, UCHIME2 showed the prevalence
327 of “fake models” or real biological sequences that can be perfectly reconstructed
328 as apparent chimeras of other sequences, which suggests that perfect chimera de-
329 tection is theoretically unattainable. UCHIME2 also introduces several preset
330 modes (e.g., denoised, balanced, sensitive, specific, high-confidence) designed to
331 tune sensitivity and specificity depending on dataset characteristics. These modes
332 allow users to adjust the algorithm to the expected noise level or analytical goals.

333 Despite these improvements, UCHIME2 must be applied with caution. The
334 author’s website manual (Edgar, n.d) explicitly advises against using UCHIME2
335 as a standalone chimera-filtering step in OTU clustering or denoising workflows
336 because doing so can inflate both false positives and false negatives.

337 2.3.3 CATch

338 As previously mentioned, UCHIME (Edgar et al., 2011) relied on alignment-based
339 sequences in amplicon data. However, researchers soon observed that different al-
340 gorithms often produced inconsistent predictions. A sequence might be identified
341 as chimeric by one tool but classified as non-chimeric by another, resulting in
342 unreliable filtering outcomes across studies.

343 To address these inconsistencies, Mysara, Saeys, Leys, Raes, and Monsieurs
344 (2015) developed the Classifier for Amplicon Tool Chimeras (CATCh), which rep-
345 resents the first ensemble machine learning system designed for chimera detection
346 in 16S rRNA amplicon sequencing. Rather than depending on a single detec-
347 tion strategy, CATCh integrates the outputs of several established tools, includ-
348 ing UCHIME, ChimeraSlayer, DECIPHER, Pintail, and Perseus. The individual
349 scores and binary decisions generated by these tools are used as input features for
350 a supervised learning model. The algorithm employs a Support Vector Machine
351 (SVM) with a Pearson VII Universal Kernel (PUK) to determine optimal weight-
352 ings among the input features and to assign each sequence a probability of being
353 chimeric.

354 Benchmarking in both reference-based and de novo modes demonstrated signif-
355 icant performance improvements. CATCh achieved sensitivities of approximately
356 85 percent in reference-based mode and 92 percent in de novo mode, with corre-
357 sponding specificities of approximately 96 percent and 95 percent. These results
358 indicate that CATCh detected 7 to 12 percent more chimeras than any individual
359 algorithm while maintaining high precision.

360 **2.3.4 ChimPipe**

361 Among the available tools for chimera detection, ChimPipe is a pipeline developed
362 to identify chimeric sequences such as biological chimeras. It uses both discordant
363 paired-end reads and split-read alignments to improve the accuracy and sensitivity
364 of detecting biological chimeras (Rodriguez-Martin et al., 2017). By combining
365 these two sources of information, ChimPipe achieves better precision than meth-
366 ods that depend on a single type of indicator.

367 The pipeline works with many eukaryotic species that have available genome
368 and annotation data (Rodriguez-Martin et al., 2017). It can also predict multiple
369 isoforms for each gene pair and identify breakpoint coordinates that are useful
370 for reconstructing and verifying chimeric transcripts. Tests using both simulated
371 and real datasets have shown that ChimPipe maintains high accuracy and reliable
372 performance.

373 ChimPipe lets users adjust parameters to fit different sequencing protocols or
374 organism characteristics. Experimental results have confirmed that many chimeric
375 transcripts detected by the tool correspond to functional fusion proteins, demon-
376 strating its utility for understanding chimera biology and its potential applications
377 in disease research (Rodriguez-Martin et al., 2017).

378 2.4 Machine Learning Approaches for Chimera

379 and Sequence Quality Detection

380 Traditional chimera detection tools rely primarily on heuristic or alignment-based
381 rules. Recent advances in machine learning (ML) have demonstrated that models
382 trained on sequence-derived features can effectively capture compositional and
383 structural patterns in biological sequences. Although most existing ML systems
384 such as those used for antibiotic resistance prediction, taxonomic classification,
385 or viral identification are not specifically designed for chimera detection, they
386 highlight how data-driven models can outperform similarity-based heuristics by
387 learning intrinsic sequence signatures. In principle, ML frameworks can integrate
388 indicators such as k-mer frequencies, GC-content variation and split-alignment
389 metrics to identify subtle anomalies that may indicate a chimeric origin (Arango
390 et al., 2018; Liang, Bible, Liu, Zou, & Wei, 2020; Ren et al., 2020).

391 2.4.1 Feature-Based Representations of Genomic Se-

392 quences

393 Feature extraction converts DNA sequences into numerical representations suit-
394 able for machine-learning models. One approach is k-mer frequency analysis,
395 which counts short nucleotide sequences within a read (Vervier, Mahé, Tournoud,
396 Veyrieras, & Vert, 2015). High-frequency k-mers, including simple repeats such
397 as “AAAAAA,” can highlight repetitive or unusual regions that may occur near
398 chimeric junctions. Comparing k-mer patterns across adjacent parts of a read can
399 help identify such regions, while GC content provides an additional descriptor of

400 local sequence composition (Ren et al., 2020).

401 Alignment-derived features further inform junction detection. Long-read tools
402 such as Sniffles (Sedlazeck et al., 2018) use split alignments to locate breakpoints
403 across extended sequences, whereas short-read aligners like Minimap2 (Li, 2018)
404 report supplementary and secondary alignments that indicate local discontinu-
405 ities. Split alignments, where parts of a read map to different regions, can reveal
406 template-switching events. These features complement k-mer profiles and en-
407 hance detection of potentially chimeric reads, even in datasets with incomplete
408 references.

409 Microhomology, or short sequences shared between adjacent segments, is an-
410 other biologically meaningful feature. Its length, typically a few to tens of base
411 pairs, has been linked to microhomology-mediated repair and template-switching
412 mechanisms (Sfeir & Symington, 2015). In PCR-induced chimeras, short iden-
413 tical sequences at junctions provide a clear signature of chimerism. Measuring
414 the longest exact overlap at each breakpoint complements k-mer and alignment
415 features and helps identify reads that are potentially chimeric.

416 2.5 Synthesis of Chimera Detection Approaches

417 To provide an integrated overview of the literature discussed in this chapter, Ta-
418 ble 2.1 summarizes the major chimera detection studies, their methodological
419 approaches, and their known limitations.

Table 2.1: Comparison of Chimera Detection Approaches and Tools

Method / Tool	Core Approach	Key Limitations
Reference-based Detection	Compares each query sequence against curated databases of verified, non-chimeric sequences; evaluates segment similarity to identify mosaic patterns.	Accuracy depends on database completeness; performs poorly for novel taxa or missing parents; limited sensitivity for low-divergence chimeras.
De novo Detection	Identifies chimeras using only internal dataset structure; leverages abundance hierarchy and compositional similarity to infer whether low-abundance sequences can be reconstructed from abundant parents.	Assumes true sequences are more abundant; fails when amplification bias distorts abundances; struggles when parental sequences are similarly abundant or highly similar.
UCHIME	Alignment-based model that partitions the query into segments, identifies parent candidates, and computes a chimera score via a three-way alignment; supports reference and de novo modes.	Reduced accuracy for very closely related parents (<0.8% divergence); sensitive to incomplete databases; de novo mode fails if parents are absent or not sufficiently more abundant.
UCHIME2	Updated UCHIME with improved benchmarking (CHSIMA) and multiple sensitivity/specificity presets; better handles incomplete references and dataset variability.	“Fake models” limit theoretical accuracy; genuine variants may mimic chimeras; not recommended as a standalone step in OTU or denoising pipelines due to increased false positives/negatives.
CATCh	First ensemble ML model for 16S chimera detection; integrates outputs of UCHIME, ChimeraSlayer, DECIPHER, Pintail, and Perseus using an SVM to boost overall prediction accuracy.	Performance constrained by underlying tools; ML model cannot capture features not present in component algorithms; may misclassify in highly novel or low-coverage datasets.
ChimPipe	Pipeline for detecting biological chimeras in RNA-seq using discordant paired-end reads and split-read alignments; identifies isoforms and breakpoint coordinates.	Requires high-quality genome and annotation; tailored to RNA-seq rather than amplicons; computationally intensive; limited to organisms with available reference genomes.

420 Across existing studies, no single approach reliably detects all forms of chimeric
421 sequences, and the reviewed literature consistently shows that chimeras remain a
422 persistent challenge in genomics and bioinformatics. Although the surveyed tools
423 are not designed specifically for organelle genome assembly, they provide valua-
424 able insights into which methodological strategies are effective and where current
425 approaches fall short. These limitations collectively define a clear research gap:
426 the need for a specialized, feature-driven detection framework tailored to PCR-
427 induced mitochondrial chimeras. Addressing this gap aligns with the research
428 objective outlined in Section 1.3, which is to develop and evaluate a machine-
429 learning-based pipeline (MitoChime) that improves the quality of downstream
430 mitochondrial genome assembly. In support of this aim, the subsequent chapters
431 describe the design, implementation, and evaluation of the proposed tool.

⁴³² Chapter 3

⁴³³ Research Methodology

⁴³⁴ This chapter outlines the steps involved in completing the study, including data
⁴³⁵ gathering, generating simulated mitochondrial Illumina reads, preprocessing and
⁴³⁶ indexing the data, developing a feature extraction pipeline to extract key features,
⁴³⁷ applying machine learning algorithms for chimera detection, and validating and
⁴³⁸ comparing model performance.

⁴³⁹ 3.1 Research Activities

⁴⁴⁰ As illustrated in Figure 3.1, this study carried out a sequence of procedures to
⁴⁴¹ detect PCR-induced chimeric reads in mitochondrial genomes. The process began
⁴⁴² with collecting a mitochondrial reference sequence of *Sardinella lemuru* from the
⁴⁴³ National Center for Biotechnology Information (NCBI) database, which was used
⁴⁴⁴ as a reference for generating simulated clean and chimeric reads. These reads
⁴⁴⁵ were subsequently indexed and mapped. The resulting collections then passed

446 through a feature extraction pipeline that extracted k-mer profiles, supplementary
447 alignment (SA) features, and microhomology information to prepare the data for
448 model construction. The machine learning model was trained using the processed
449 input, and its precision and accuracy were assessed. It underwent tuning until it
450 reached the desired performance threshold, after which it proceeded to validation
451 and will undergo testing.

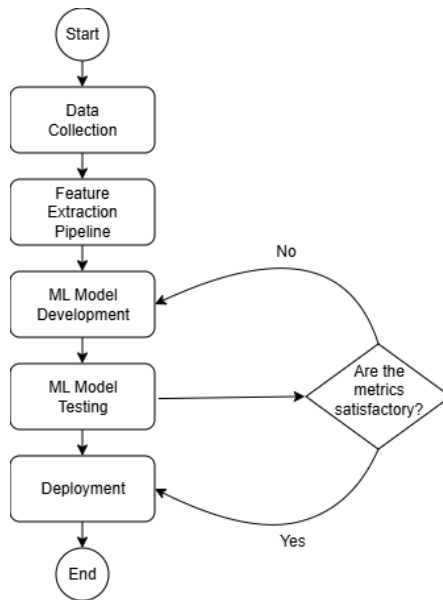


Figure 3.1: Process Diagram of Special Project

452 3.1.1 Data Collection

453 The mitochondrial genome reference sequence of *S. lemuru* was obtained from the
454 NCBI database (accession number NC_039553.1) in FASTA format. This sequence
455 served as the basis for generating simulated reads for model development.

456 This step was scheduled to begin in the first week of November 2025 and
457 expected to be completed by the end of that week, with a total duration of ap-

458 proximately one (1) week.

459 **Data Preprocessing**

460 To reduce manual repetition, all steps in the simulation and preprocessing pipeline
461 were executed using a custom script in Python (Version 3.11). The script runs
462 each stage, including read simulation, reference indexing, mapping, and alignment
463 processing, in a fixed sequence.

464 Sequencing data were simulated from the NCBI reference genome using `wgsim`
465 (Version 1.13). First, a total of 10,000 paired-end fragments were simulated,
466 producing 20,000 reads (10,000 forward and 10,000 reverse) from the the original
467 reference (`original_reference.fasta`) and and designated as clean reads using
468 the command:

```
469 wgsim -1 150 -2 150 -r 0 -R 0 -X 0 -e 0.001 -N 10000 \  
470     original_reference.fasta ref1.fastq ref2.fastq
```

471 The command parameters are as follows:

- 472 • `-1` and `-2`: read lengths of 150 base pairs for each paired-end read.
- 473 • `-r`, `-R`, `-X`: mutation rate, fraction of indels, and indel extension probability,
474 all set to a default value of 0.
- 475 • `-e`: base error rate, set to 0.001 to simulate realistic sequencing errors.
- 476 • `-N`: number of read pairs, set to 10,000.

477 Chimeric sequences were then generated from the same NCBI reference using a
478 separate Python script. Two non-adjacent segments were randomly selected such
479 that their midpoint distances fell within specified minimum and maximum thresh-
480 olds. The script attempts to retain microhomology, or short identical sequences
481 at segment junctions, to mimic PCR-induced template switching. The resulting
482 chimeras were written to `chimera_reference.fasta`, with headers recording seg-
483 ment positions and microhomology length. The `chimera_reference.fasta` was
484 processed with `wgsim` to simulate 10,000 paired-end fragments, generating 20,000
485 chimeric reads (10,000 forward reads in `chimeric1.fastq` and 10,000 reverse reads
486 in `chimeric2.fastq`) using the command format.

487 Next, a `minimap2` index of the reference genome was created using:

```
488 minimap2 -d ref.mmi original_reference.fasta
```

489 Minimap2 (Version 2.28) is a tool used to map reads to a reference genome.
490 The index `ref.mmi` of the original reference sequence is required by `minimap2` for
491 efficient read mapping. Mapping allows extraction of alignment features from each
492 read, which were used as input for the machine learning model. The simulated
493 clean and chimeric reads were then mapped to the reference index as follows:

```
494 minimap2 -ax sr -t 8 ref.mmi ref1.fastq ref2.fastq > clean.sam
```

```
495 minimap2 -ax sr -t 8 ref.mmi \  
496 chimeric1.fastq chimeric2.fastq > chimeric.sam
```

497 Here, `-ax sr` specifies short-read alignment mode, and `-t 8` uses 8 CPU

498 threads. The resulting clean and chimeric SAM files contain the alignment posi-
499 tions of each read relative to the original reference genome.

500 The SAM files were then converted to BAM format, sorted, and indexed using

501 `samtools` (Version 1.20):

```
502 samtools view -bS clean.sam -o clean.bam  
503 samtools view -bS chimeric.sam -o chimeric.bam  
504  
505 samtools sort clean.bam -o clean.sorted.bam  
506 samtools index clean.sorted.bam  
507  
508 samtools sort chimeric.bam -o chimeric.sorted.bam  
509 samtools index chimeric.sorted.bam
```

510 BAM files are the compressed binary version of SAM files, which enables faster
511 processing and reduced storage. Sorting arranges reads by genomic coordinates,
512 and indexing allows detection of SA as a feature for the machine learning model.

513 The total number of simulated reads was expected to be 40,000. The final col-
514 lection of reads contained 19,984 clean reads and 20,000 chimeric reads (39,984 en-
515 tries in total), providing a roughly balanced distribution between the two classes.
516 After alignment with `minimap2`, only 19,984 clean reads remained because un-
517 mapped reads were not included in the BAM file. Some sequences failed to align
518 due to the 5% error rate defined during `wgsim` simulation, which produced mis-
519 matches that caused certain reads to fall below the aligner's matching threshold.

520 This whole process is scheduled to start in the second week of November 2025

521 and is expected to be completed by the last week of November 2025, with a total
522 duration of approximately three (3) weeks.

523 3.1.2 Feature Extraction Pipeline

524 This stage directly follows the previous alignment phase, utilizing the resulting
525 BAM files (specifically `chimeric.sorted.bam` and `clean.sorted.bam`). A custom
526 Python script was created to efficiently process each primary-mapped read to
527 extract the necessary set of analytical features, which are then compiled into a
528 structured feature matrix in TSV format. The pipeline's core functionality relies
529 on libraries, namely `Pysam` (Version 0.22) for the robust parsing of BAM structures
530 and `NumPy` (Version 1.26) for array operations and computations. The pipeline
531 focuses on three principal features that collectively capture biological signatures
532 associated with PCR-induced chimeras: (1) Supplementary alignment flag (SA
533 count), (2) k-mer composition difference, and (3) microhomology.

534 Supplementary Alignment Flag

535 Split-alignment information was derived from the `SA` (Supplementary Alignment)
536 tag embedded in each primary read of the BAM file. This tag is typically asso-
537 ciated with reads that map to multiple genomic locations, suggesting a chimeric
538 structure. To extract this information, the script first checked whether the read
539 carried an `SA:Z` tag. If present, the tag string was parsed using the function
540 `parse_sa_tag`, yielding a structure for each alignment containing the reference
541 name, mapped position, strand, mapping quality, and number of mismatches.

542 After parsing, the function `sa_feature_stats` was applied to establish the fun-
543 damental split indicators, `has_sa` and `sa_count`. Along with these initial counts,
544 the function synthesized a summarization by aggregating metrics related to the
545 structure and reliability of the split alignments.

546 **K-mer Composition Difference**

547 Chimeric reads often comprise fragments from distinct genomic regions, resulting
548 in a compositional discontinuity between segments. Comparing k-mer frequency
549 profiles between the left and right halves of a read allows for the detection of such
550 abrupt compositional shifts, independent of alignment information.

551 The script implemented this by inferring a likely junction breakpoint using
552 the function `infer_breakpoints`, prioritizing the boundaries defined by soft-
553 clipping operations in the CIGAR string. If no clipping was present, the midpoint
554 of the alignment or the read length was utilized as a fallback. The read sequence
555 was then divided into left and right segments at this inferred breakpoint, and
556 k-mer frequency profiles ($k = 5$) were generated for both halves, ignoring any
557 k-mers containing ambiguous 'N' bases. The resulting k-mer frequency vectors
558 will be normalized and compared using the functions `cosine_difference` and
559 `js_divergence`.

560 **Microhomology**

561 The workflow for extracting the microhomology feature also started by utilizing
562 the `infer_breakpoints` similar to the k-mer workflow. Once a breakpoint was es-

563 established, the script scanned a ± 40 base pair window surrounding the breakpoint
564 and used the function `longest_suffix_prefix_overlap` to identify the longest
565 exact suffix-prefix overlap between the left and right read segments. This overlap,
566 which represents consecutive bases shared at the junction, was recorded as the
567 `microhomology_length` in the dataset. The 40-base pair window was chosen to
568 ensure that short shared sequences at or near the breakpoint were captured, with-
569 out including distant sequences that are unrelated. Additionally, the GC content
570 of the overlapping sequence was calculated using the function `gc_content`, which
571 counts guanine (G) and cytosine (C) bases within the detected microhomology
572 and divides by the total length, yielding a proportion between 0 and 1, and was
573 stored under the `microhomology_gc` attribute. Short microhomologies, typically
574 3-20 base pairs in length, are recognized signatures of PCR-induced template
575 switching (Peccoud et al., 2018).

576 A k-mer length of 6 was used to capture patterns within the same 40-base pair
577 window surrounding each breakpoint. These profiles complement microhomology
578 measurements and help identify junctions that are potentially chimeric.

579 To ensure correctness and adherence to best practices, bioinformatics experts
580 at the PGC Visayas will be consulted to validate the pipeline design, feature
581 extraction logic, and overall data integrity. This stage of the study was scheduled
582 to begin in the third week of November 2025 and conclude by the first week
583 of December 2025, with an estimated total duration of approximately three (3)
584 weeks.

585 **3.1.3 Machine Learning Model Development**

586 After feature extraction, the per-read feature matrices for clean and chimeric
587 reads were merged into a single dataset. Each row corresponded to one paired-
588 end read, and columns encoded alignment-structure features (e.g., supplementary
589 alignment count and spacing between segments), CIGAR-derived soft-clipping
590 statistics (e.g., left and right soft-clipped length, total clipped bases), k-mer com-
591 position discontinuity between read segments, and microhomology descriptors
592 near candidate junctions. The resulting feature set was restricted to quantities
593 that can be computed from standard BAM/FASTQ files in typical mitochondrial
594 sequencing workflows.

595 The labelled dataset was randomly partitioned into training (80%) and test
596 (20%) subsets using stratified sampling to preserve the 1:1 ratio of clean to
597 chimeric reads. Model development and evaluation were implemented in Python
598 (Version 3.11) using the `scikit-learn`, `xgboost`, `lightgbm`, and `catboost` li-
599 braries. A broad panel of classification algorithms was then benchmarked on the
600 training data to obtain a fair comparison of different model families under identical
601 feature conditions. The panel included: a trivial dummy classifier, L2-regularized
602 logistic regression, a calibrated linear support vector machine (SVM), k -nearest
603 neighbours, Gaussian Naïve Bayes, decision-tree ensembles (Random Forest, Ex-
604 tremely Randomized Trees, and Bagging with decision trees), gradient boosting
605 methods (Gradient Boosting, XGBoost, LightGBM, and CatBoost), and a shallow
606 multilayer perceptron (MLP).

607 For each model, five-fold stratified cross-validation was performed on the train-
608 ing set. In every fold, four-fifths of the data were used for fitting and the remaining

609 one-fifth for validation. Mean cross-validation accuracy, precision, recall, F1-score
610 for the chimeric class, and area under the receiver operating characteristic curve
611 (ROC–AUC) were computed to summarize performance and rank candidate meth-
612 ods. This baseline screen allowed comparison of linear, probabilistic, neural, and
613 ensemble-based approaches and identified tree-based ensemble and boosting mod-
614 els as consistently strong performers relative to simpler baselines.

615 **3.1.4 Model Benchmarking, Hyperparameter Optimiza-
616 tion, and Evaluation**

617 Model selection and refinement proceeded in two stages. First, the cross-validation
618 results from the broad panel were used to identify a subset of competitive mod-
619 els for more detailed optimization. Specifically, ten model families were carried
620 forward: L2-regularized logistic regression, calibrated linear SVM, Random For-
621 est, ExtraTrees, Gradient Boosting, XGBoost, LightGBM, CatBoost, Bagging
622 with decision trees, and a shallow MLP. This subset spans both linear and non-
623 linear decision boundaries, but emphasizes ensemble and boosting methods, which
624 showed superior F1 and ROC–AUC in the initial benchmark.

625 Second, hyperparameter optimization was conducted for each of the ten se-
626 lected models using randomized search with five-fold stratified cross-validation
627 (`RandomizedSearchCV`). For tree-based ensembles, the search space included the
628 number of trees, maximum depth, minimum samples per split and leaf, and the
629 fraction of features considered at each split. For boosting methods, key hyper-
630 parameters such as the number of boosting iterations, learning rate, tree depth,
631 subsampling rate, and column subsampling rate were tuned. For the MLP, the

632 number and size of hidden layers, learning rate, and L_2 regularization strength
633 were varied. In all cases, the primary optimisation criterion was the F1-score of
634 the chimeric class, averaged across folds.

635 For each model family, the hyperparameter configuration with the highest
636 mean cross-validation F1-score was selected as the best-tuned estimator. These
637 tuned models were then refitted on the full training set and evaluated once on the
638 held-out test set to obtain unbiased estimates of performance. Test-set metrics in-
639 cluded accuracy, precision, recall, F1-score for the chimeric class, and ROC–AUC.
640 Confusion matrices and ROC curves were generated for the top-performing mod-
641 els to characterise common error modes, such as false negatives (missed chimeric
642 reads) and false positives (clean reads incorrectly labelled as chimeric). The final
643 model or small set of models for downstream interpretation was chosen based on
644 a combination of test-set F1-score, ROC–AUC, and practical considerations such
645 as model complexity and ease of deployment within a feature extraction pipeline.

646 3.1.5 Feature Importance and Interpretation

647 To relate model decisions to biologically meaningful signals, feature-importance
648 analyses were performed on the best-performing tree-based models. Two comple-
649 mentary approaches were used. First, built-in importance measures from ensemble
650 methods (e.g., split-based importances in Random Forest and Gradient Boosting)
651 were examined to obtain an initial ranking of features based on their contribution
652 to reducing impurity. Second, model-agnostic permutation importance was com-
653 puted on the test set by repeatedly permuting each feature column while keeping
654 all others fixed and measuring the resulting decrease in F1-score. Features whose

655 permutation led to a larger performance drop were interpreted as more influential
656 for chimera detection.

657 For interpretability, individual features were grouped into four conceptual
658 families: (i) supplementary alignment and alignment-structure features (e.g., SA
659 count, spacing between alignment segments, strand consistency), (ii) CIGAR-
660 derived soft-clipping features (e.g., left and right soft-clipped length, total clipped
661 bases), (iii) k-mer composition discontinuity features (e.g., cosine distance and
662 Jensen–Shannon divergence between k-mer profiles of read segments), and (iv) mi-
663 crohomology descriptors (e.g., microhomology length and local GC content around
664 putative breakpoints). Aggregating permutation importance scores within each
665 family allowed assessment of which biological signatures contributed most strongly
666 to the classifier’s performance. This analysis provided a basis for interpreting the
667 trained models in terms of known mechanisms of PCR-induced template switching
668 and for identifying which alignment- and sequence-derived cues are most informa-
669 tive for distinguishing chimeric from clean mitochondrial reads.

670 3.1.6 Validation and Testing

671 Validation will involve both internal and external evaluations. Internal valida-
672 tion was achieved through five-fold cross-validation on the training data to verify
673 model generalization and reduce variance due to random sampling. External vali-
674 dation will be achieved through testing on the 20% hold-out dataset derived from
675 the simulated reads, which will be an unbiased benchmark to evaluate how well
676 the trained models generalized to unseen data. All feature extraction and prepro-
677 cessing steps were performed using the same feature extraction pipeline to ensure

678 consistency and comparability across validation stages.

679 Comparative evaluation was performed across all candidate algorithms, in-
680 cluding a trivial dummy classifier, L2-regularized logistic regression, a calibrated
681 linear SVM, k-nearest neighbours, Gaussian Naïve Bayes, decision-tree ensembles,
682 gradient boosting methods, and a shallow MLP. This evaluation determined which
683 models demonstrated the highest predictive performance and computational effi-
684 ciency under identical data conditions. Their metrics were compared to identify
685 which algorithms were most suitable for further refinement.

686 3.1.7 Documentation

687 Comprehensive documentation was maintained throughout the study to ensure
688 transparency and reproducibility. All stages of the research, including data gath-
689 ering, preprocessing, feature extraction, model training, and validation, were sys-
690 tematically recorded in a `.README` file in the GitHub repository. For each ana-
691 lytical step, the corresponding parameters, software versions, and command line
692 scripts were documented to enable exact replication of results.

693 The repository structure followed standard research data management prac-
694 tices, with clear directories for datasets and scripts. Computational environments
695 were standardized using Conda, with an environment file (`environment.arm.yml`)
696 specifying dependencies and package versions to maintain consistency across sys-
697 tems.

698 For manuscript preparation and supplementary materials, Overleaf (L^AT_EX)
699 was used to produce publication-quality formatting and consistent referencing. f

700 3.2 Calendar of Activities

701 Table 3.1 presents the project timeline in the form of a Gantt chart, where each
702 bullet point corresponds to approximately one week of planned activity.

Table 3.1: Timetable of Activities

Activities (2025)	Nov	Dec	Jan	Feb	Mar	Apr	May
Data Collection and Simulation	• • •						
Feature Extraction Pipeline	• •	•					
Machine Learning Development			• •	• • •	• • •	• •	
Testing and Validation						• •	• • •
Documentation	• • •	• • •	• • •	• • •	• • •	• • •	• • •

703 **Chapter 4**

704 **Results and Discussion**

705 **4.1 Descriptive Analysis of Features**

706 This chapter presents the performance of the proposed feature set and machine-
707 learning models for detecting PCR-induced chimeric reads in simulated mitochon-
708 drial Illumina data. We first describe the behaviour of the main features, then
709 compare baseline classifiers, assess the effect of hyperparameter tuning, and fi-
710 nally analyse feature importance in terms of individual variables and biologically
711 motivated feature families.

712 The final dataset contained 31,986 reads for training and 7,997 reads for test-
713 ing, with classes balanced (approximately 4,000 clean and 4,000 chimeric reads in
714 the test split).

715 4.1.1 Univariate Distributions

716 The kernel density plots in Figures 4.1a–4.1f collectively show that alignment-
717 based features provide the strongest separation between clean and chimeric reads.
718 The distribution of `sa_count` (Figure 4.1a) is distinctly bimodal, with clean reads
719 concentrated near zero and chimeric reads peaking around one, reflecting the
720 frequent presence of supplementary alignments in chimeras. A similar pattern of
721 clear separation is observed in `softclip_left` and `softclip_right` (Figures 4.1c
722 and 4.1d), where clean reads cluster tightly at zero while chimeric reads display
723 broad, long-tailed distributions, consistent with extensive soft clipping when
724 a read spans multiple genomic locations. In contrast, `microhomology_length`
725 (Figure 4.1b) shows substantial overlap between classes, with both distribu-
726 tions sharply concentrated near zero and exhibiting smaller secondary peaks
727 at short integer lengths, indicating limited discriminative value under the sim-
728 ulated conditions. Finally, the k-mer-based features `kmer_js_divergence` and
729 `kmer_cosine_diff` (Figures 4.1e and 4.1f) exhibit highly overlapping, multimodal
730 distributions with both classes peaking near 1.0; although chimeric reads appear
731 slightly less concentrated at the highest similarity values, the separation is weak
732 overall.

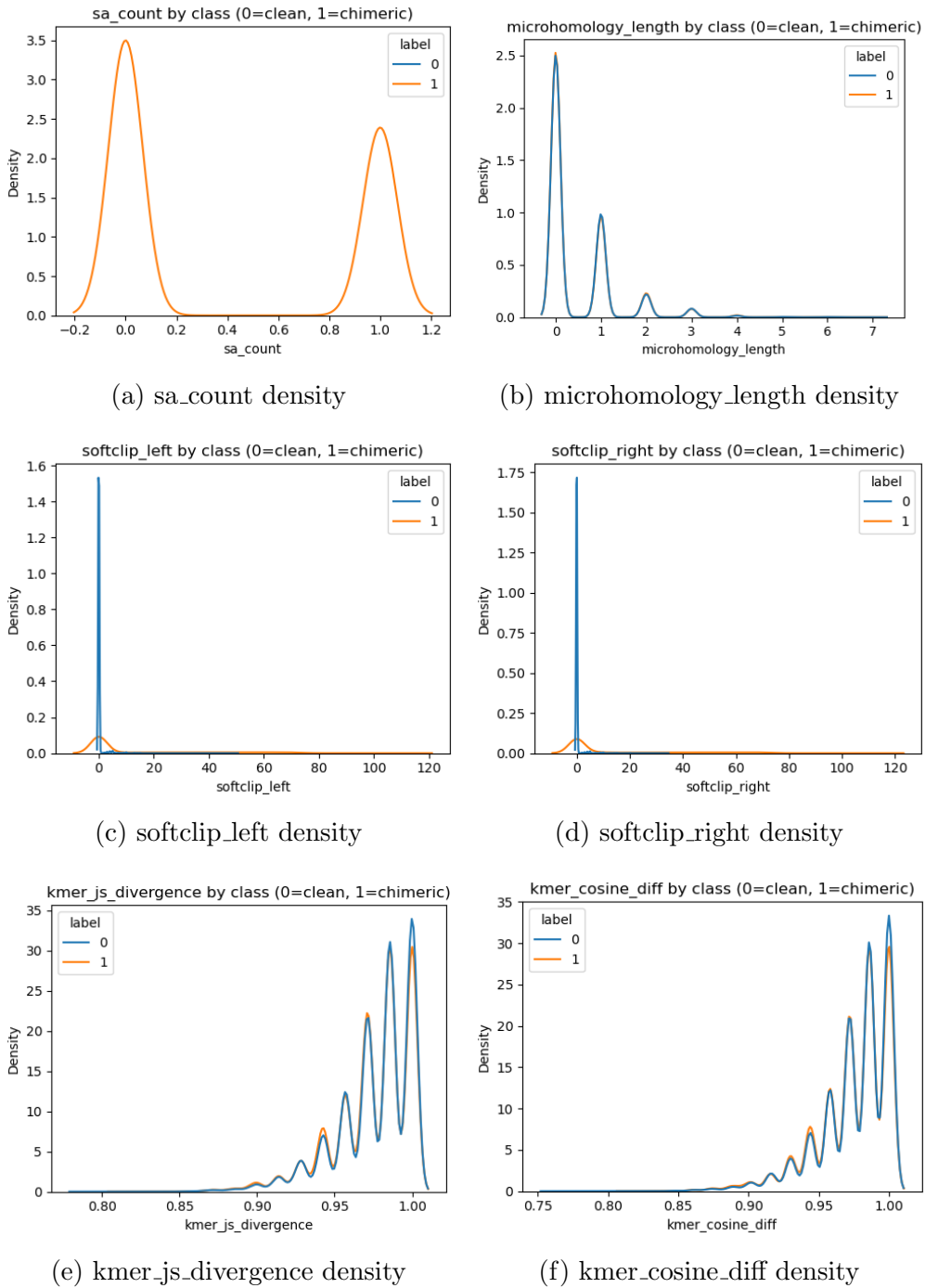


Figure 4.1: Kernel density plots of six key features comparing clean and chimeric reads.

733 4.2 Baseline Classification Performance

734 Table 4.1 summarises the performance of eleven classifiers trained on the engi-
735 neered feature set using five-fold cross-validation and evaluated on the held-out
736 test set. All models were optimised using default hyperparameters, without ded-
737 icated tuning.

738 The dummy baseline, which always predicts the same class regardless of the
739 input features, achieved an accuracy of 0.50 and test F1-score of 0.67. This re-
740 flects the balanced class distribution and provides a lower bound for meaningful
741 performance.

742 Across other models, test F1-scores clustered in a narrow band between ap-
743 proximately 0.74 and 0.77 and ROC–AUC values between 0.82 and 0.84. Gradi-
744 ent boosting, CatBoost, LightGBM, XGBoost, bagging trees, random forest, and
745 multilayer perceptron (MLP) all produced very similar scores, with CatBoost and
746 gradient boosting slightly ahead (test F1 \approx 0.77, ROC–AUC \approx 0.84). Linear
747 models (logistic regression and calibrated linear SVM) performed only marginally
748 worse (test F1 \approx 0.74), while Gaussian Naive Bayes lagged behind with substan-
749 tially lower F1 (\approx 0.65) despite very high precision for the chimeric class.

Table 4.1: Performance of baseline classifiers on the held-out test set.

model	test_accuracy	test_precision	test_recall	test_f1	test_roc_auc
dummy_baseline	0.500000	0.500000	1.000000	0.667000	0.500000
logreg_l2	0.789000	0.945000	0.614000	0.744000	0.821000
linear_svm_calibrated	0.789000	0.945000	0.614000	0.744000	0.820000
random_forest	0.788000	0.894000	0.654000	0.755000	0.834000
extra_trees	0.788000	0.901000	0.647000	0.753000	0.824000
gradient_boosting	0.802000	0.936000	0.648000	0.766000	0.840000
xgboost	0.800000	0.929000	0.650000	0.765000	0.839000
lightgbm	0.799000	0.926000	0.650000	0.764000	0.838000
catboost	0.803000	0.936000	0.650000	0.767000	0.839000
knn	0.782000	0.892000	0.642000	0.747000	0.815000
gaussian_nb	0.741000	0.996000	0.483000	0.651000	0.819000
bagging_trees	0.792000	0.900000	0.657000	0.760000	0.837000
mlp	0.789000	0.931000	0.625000	0.748000	0.819000

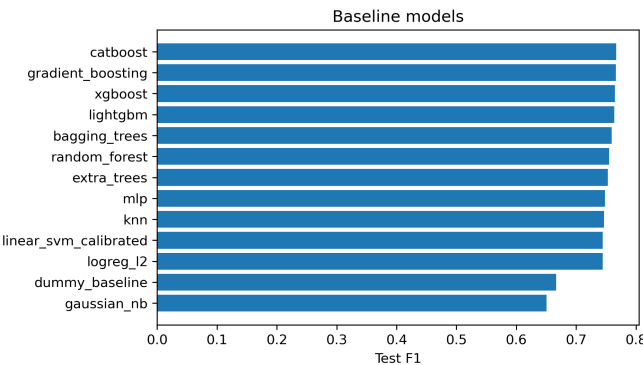


Figure 4.2: Test F1 of all baseline classifiers, showing that no single model clearly dominates and several achieve comparable performance.

750 4.3 Effect of Hyperparameter Tuning

751 To assess whether performance could be improved further, ten model families un-
 752 derwent randomised hyperparameter search (Chapter 3). The tuned metrics are
 753 summarised in Table 4.2. Overall, tuning yielded modest but consistent gains for
 754 tree-based ensembles and boosting methods, while leaving linear models essen-

755 tially unchanged or slightly worse.

756 CatBoost, gradient boosting, LightGBM, XGBoost, random forest, bagging
757 trees, and MLP all experienced small increases in test F1 (typically $\Delta F1 \approx 0.002$ –
758 0.009) and ROC–AUC (up to $\Delta AUC \approx 0.008$). After tuning, CatBoost remained
759 the best performer with test accuracy 0.802, precision 0.924, recall 0.658, F1-score
760 0.769, and ROC–AUC 0.844. Gradient boosting achieved almost identical perfor-
761 mance (F1 0.767, AUC 0.843). Random forest and bagging trees also improved
762 to F1 scores around 0.763 with AUC ≈ 0.842 .

Table 4.2: Performance of tuned classifiers on the held-out test set.

model	test_accuracy	test_precision	test_recall	test_f1	test_roc_auc
logreg_l2_tuned	0.788000	0.946000	0.612000	0.743000	0.818000
linear_svm_calibrated_tuned	0.788000	0.944000	0.612000	0.743000	0.818000
random_forest_tuned	0.797000	0.915000	0.655000	0.763000	0.842000
extra_trees_tuned	0.794000	0.910000	0.652000	0.760000	0.837000
gradient_boosting_tuned	0.802000	0.928000	0.654000	0.767000	0.843000
xgboost_tuned	0.799000	0.922000	0.653000	0.765000	0.839000
lightgbm_tuned	0.801000	0.930000	0.651000	0.766000	0.842000
catboost_tuned	0.802000	0.924000	0.658000	0.769000	0.844000
bagging_trees_tuned	0.798000	0.922000	0.650000	0.763000	0.842000
mlp_tuned	0.790000	0.934000	0.625000	0.749000	0.821000

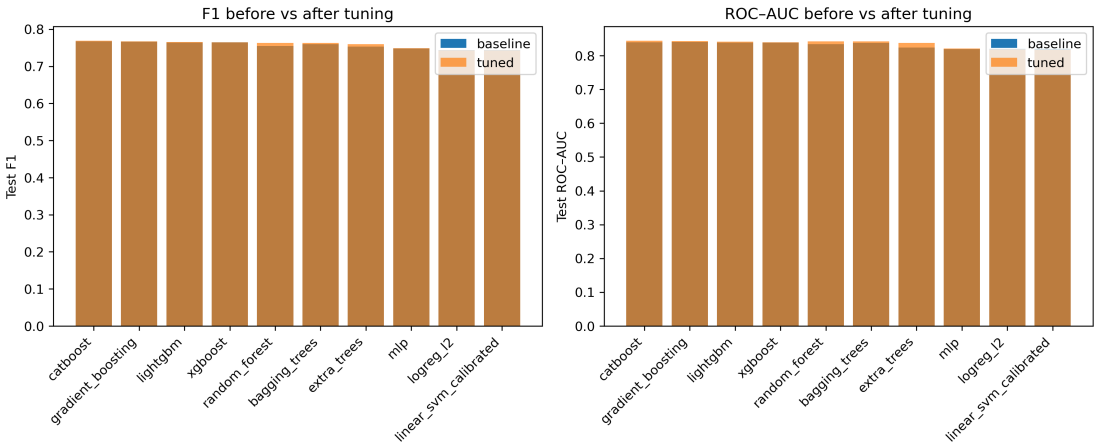


Figure 4.3: Comparison of test F1 (left) and ROC–AUC (right) for baseline and tuned models. Hyperparameter tuning yields small but consistent gains, particularly for tree-based ensembles.

763 Because improvements are small and within cross-validation variability, we
 764 interpret tuning as stabilising and slightly refining the models rather than funda-
 765 mentally altering their behaviour or their relative ranking.

766 4.4 Detailed Evaluation of Representative Mod- 767 els

768 For interpretability and diversity, four tuned models were selected for deeper
 769 analysis: CatBoost (best-performing boosted tree), scikit-learn gradient boost-
 770 ing (canonical gradient-boosting implementation), random forest (non-boosted
 771 ensemble baseline), and L2-regularised logistic regression (linear baseline). All
 772 models were trained on the engineered feature set and evaluated on the same
 773 held-out test data.

774 4.4.1 Confusion Matrices and Error Patterns

775 Classification reports and confusion matrices for the four models reveal consistent
776 patterns. CatBoost and gradient boosting both reached overall accuracy of ap-
777 proximately 0.80 with similar macro-averaged F1 scores (~ 0.80). For CatBoost,
778 precision and recall for clean reads were 0.73 and 0.95, respectively, while for
779 chimeric reads they were 0.92 and 0.66 ($F1 = 0.77$). Gradient boosting showed
780 nearly identical trade-offs.

781 Random forest attained slightly lower accuracy (0.80) and chimeric F1 (0.76),
782 whereas logistic regression achieved the lowest accuracy among the four (0.79)
783 and chimeric F1 (0.74), although it provided the highest chimeric precision (0.95)
784 at the cost of lower recall (0.61).

785 Across all models, errors were asymmetric. False negatives (chimeric reads
786 predicted as clean) were more frequent than false positives. For example, CatBoost
787 misclassified 1 369 chimeric reads as clean but only 215 clean reads as chimeric.
788 This pattern indicates that the models are conservative: they prioritise avoiding
789 spurious chimera calls at the expense of missing some true chimeras. Depending on
790 downstream application, alternative decision thresholds or cost-sensitive training
791 could be explored to adjust this balance.

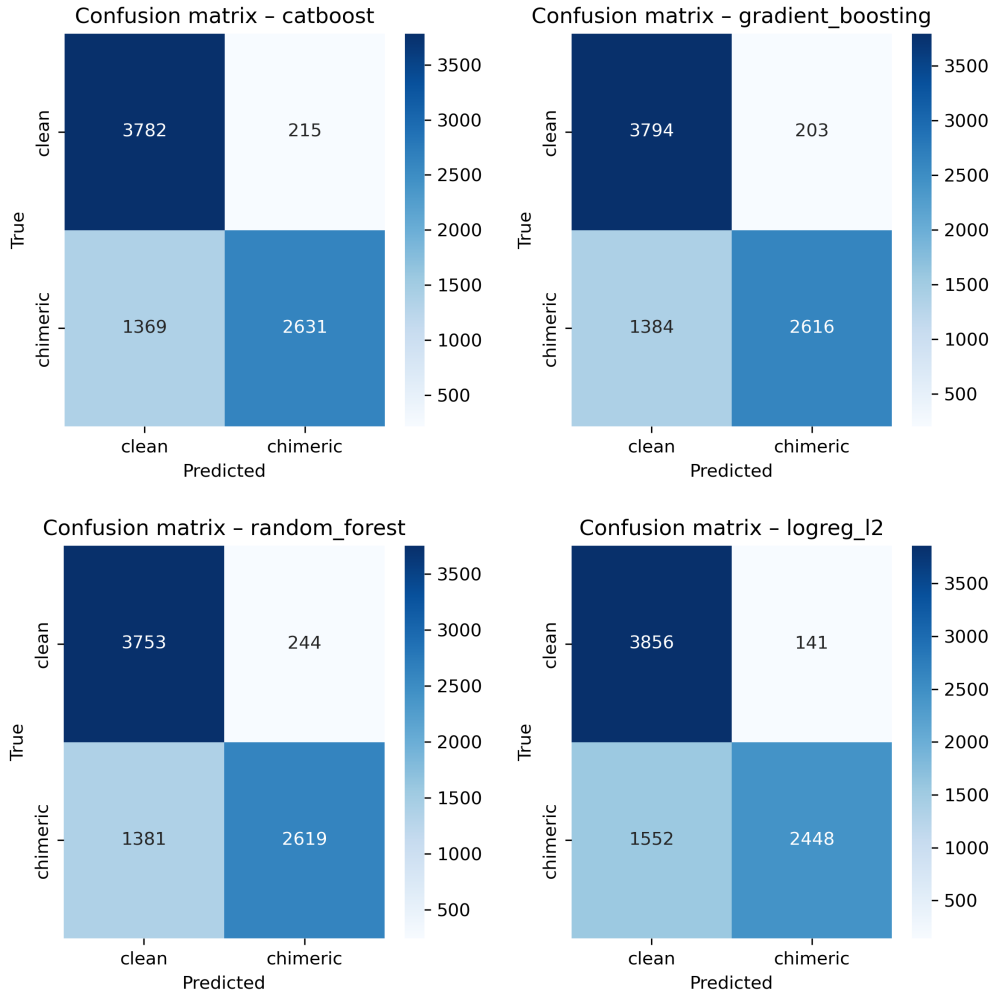


Figure 4.4: Confusion matrices for the four representative models on the held-out test set. All models show more false negatives (chimeric reads called clean) than false positives.

792 4.4.2 ROC and Precision–Recall Curves

793 Receiver operating characteristic (ROC) and precision–recall (PR) curves (Figure 4.5) further support the similarity among the top models. The three tree-based
 794 ensembles (CatBoost, gradient boosting, random forest) achieved ROC–AUC val-
 795 ues of approximately 0.84 and average precision (AP) around 0.88. Logistic re-

797 gression performed slightly worse ($AUC \approx 0.82$, $AP \approx 0.87$) but still substantially
798 better than random guessing.

799 The PR curves show that precision remains above 0.9 across a broad range
800 of recall values (up to roughly 0.5–0.6), after which precision gradually declines.
801 This behaviour indicates that the models can assign very high confidence to a
802 subset of chimeric reads, while more ambiguous reads can only be recovered by
803 accepting lower precision.

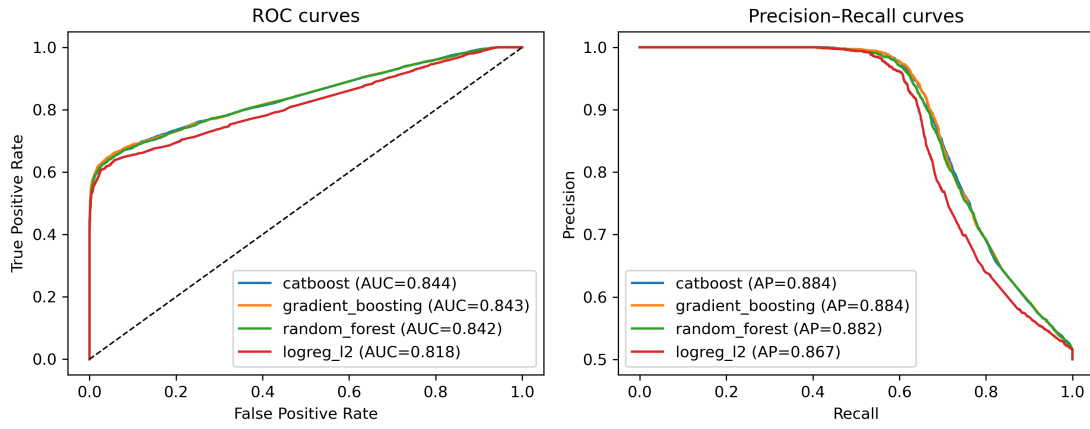


Figure 4.5: ROC (left) and precision–recall (right) curves for the four representative models on the held-out test set. Tree-based ensembles cluster closely, with logistic regression performing slightly but consistently worse.

804 **4.5 Feature Importance and Biological Interpre-**
805 **tation**

806 **4.5.1 Permutation Importance of Individual Features**

807 To understand how each classifier made predictions, feature importance was quan-
808 tified using permutation importance. In this approach, the values of a single fea-
809 ture are randomly shuffled, and the resulting drop in F_1 score (ΔF_1) reflects how
810 strongly the model depends on that feature. Greater decreases in F_1 indicate
811 stronger reliance on that feature. This analysis was applied to four representa-
812 tive models: CatBoost, Gradient Boosting, Random Forest, and L_2 -regularized
813 Logistic Regression.

814 As shown in Figure 4.6, the total number of clipped bases consistently pro-
815 vides a strong predictive signal, particularly in Random Forest, Gradient Boosting,
816 and L_2 -regularized Logistic Regression. CatBoost differs by assigning the highest
817 importance to k-mer divergence metrics such as `kmer_js_divergence`, which cap-
818 ture subtle sequence changes resulting from structural variants or PCR-induced
819 chimeras. Soft-clipping features (`softclip_left` and `softclip_right`) provide
820 additional context around breakpoints, complementing these primary signals in
821 all models except Gradient Boosting. L_2 -regularized Logistic Regression relies
822 more on alignment-based split-read metrics when breakpoints are simple, but it is
823 less effective at detecting complex rearrangements that introduce novel sequences.

824 Overall, these results indicate that accurate detection of chimeric reads relies
825 on both alignment-based signals and k-mer compositional information. Explicit

826 microhomology features contribute minimally in this analysis, and combining both
 827 alignment-based and sequence-level features enhances model sensitivity and speci-
 828 ficity.

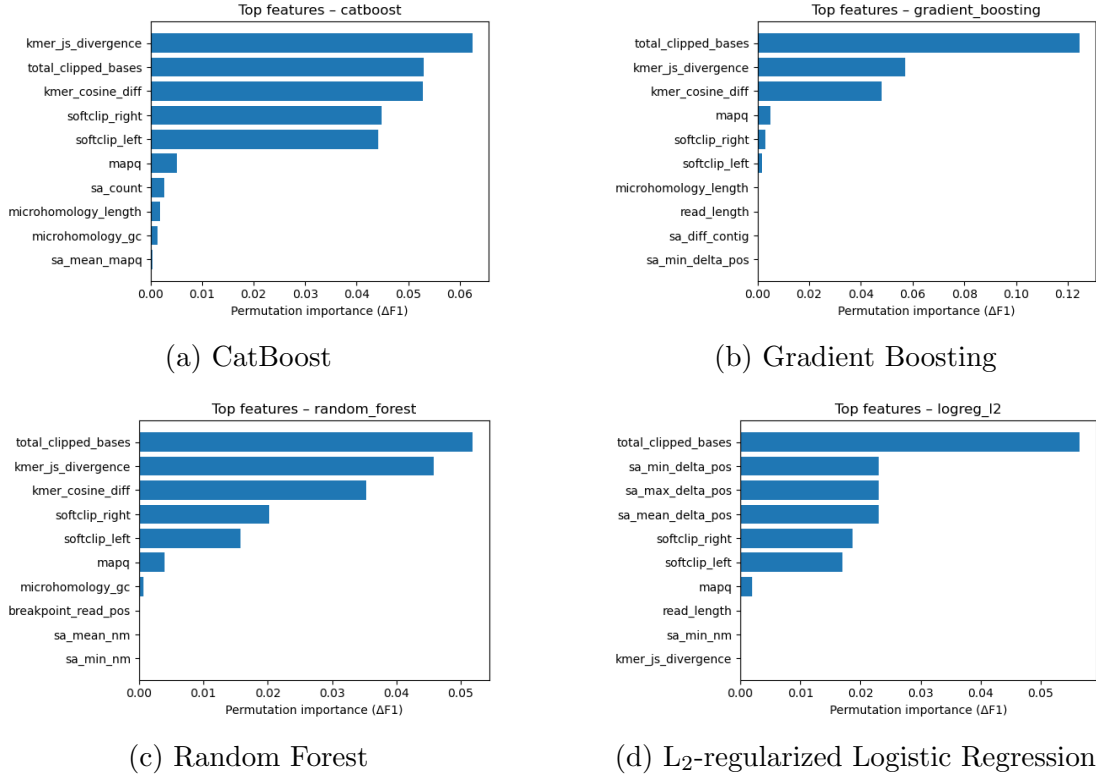


Figure 4.6: Permutation-based feature importance for four representative classifiers. Clipping and k-mer composition features are generally the strongest predictors, whereas microhomology and other alignment metrics contribute minimally.

829 4.5.2 Feature Family Importance

830 To evaluate the contribution of broader biological signals, features were
 831 grouped into five families: SA_structure (supplementary alignment and seg-
 832 ment metrics, e.g., has_sa, sa_count, sa_min_delta_pos, sa_mean_nm), Clipping
 833 (softclip_left, softclip_right, total_clipped_bases, breakpoint_read_pos),

834 Kmer_jump (`kmer_cosine_diff`, `kmer_js_divergence`), Micro_homology, and
835 Other (e.g., `mapq`).

836 Aggregated analyses reveal consistent patterns across models. In CatBoost,
837 the Clipping family has the largest cumulative contribution (0.14), followed
838 by Kmer_jump (0.12), with Other features contributing modestly (0.005) and
839 SA_structure (0.003) and Micro_homology (0.003) providing minimal predictive
840 power. Gradient Boosting shows a similar trend, with Clipping (0.13) domi-
841 nating, Kmer_jump (0.11) secondary, and the remaining families contributing
842 negligibly. Random Forest integrates both Clipping (0.088) and Kmer_jump
843 (0.08) effectively, while SA_structure, Micro_homology, and Other remain minor
844 contributors. L₂-regularized Logistic Regression emphasizes Clipping (0.09)
845 and SA_structure (0.07), with Kmer_jump and Micro_homology having minimal
846 impact.

847 Both feature-level and aggregated analyses indicate that detection of chimeric
848 reads in this dataset relies primarily on alignment disruptions (Clipping) and
849 k-mer compositional shifts (Kmer_jump), which often arise from PCR-induced
850 recombination events, while explicit microhomology features contribute minimally.

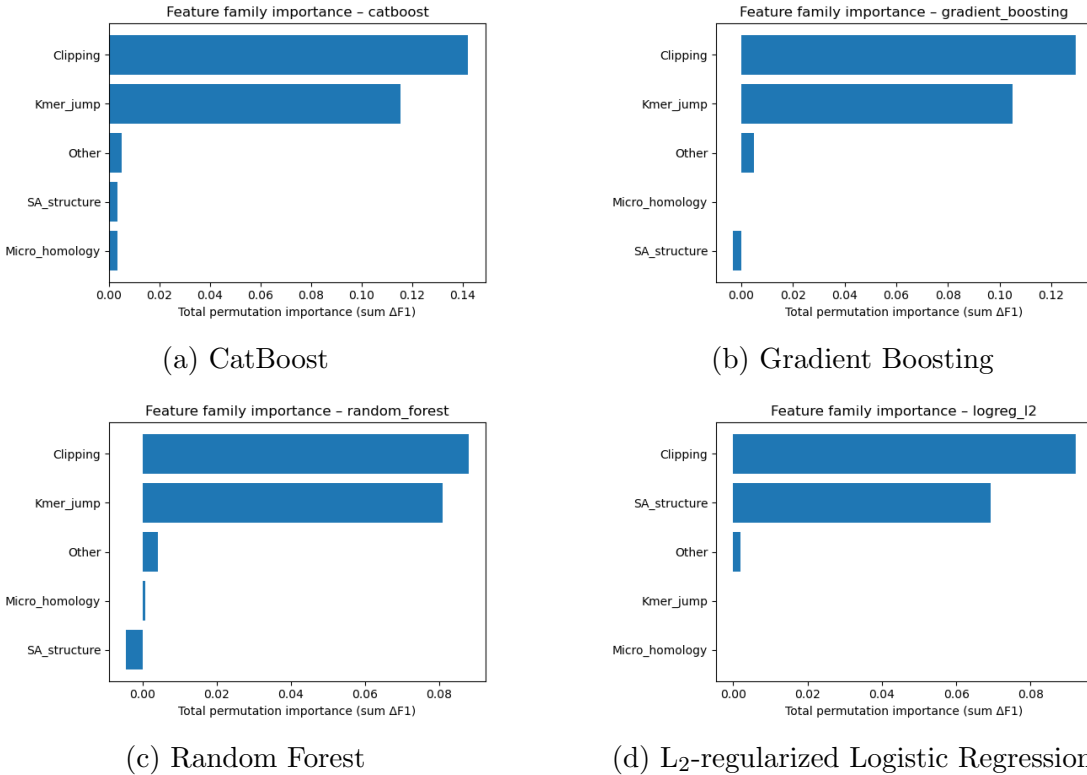


Figure 4.7: Aggregated feature family importance across four models. Clipping and k-mer compositional shifts are consistently the dominant contributors, while SA_structure, Micro_homology, and other features contribute minimally.

851 4.6 Summary of Findings

852 After removing trivially discriminative metadata, all models performed substan-
 853 tially better than the dummy baseline, with test F1-scores around 0.76 and ROC-
 854 AUC values near 0.84. Hyperparameter tuning yielded modest improvements,
 855 with boosting methods, particularly CatBoost and gradient boosting, achieving
 856 the highest performance. Confusion matrices and precision-recall curves indicate
 857 that these models prioritise precision for chimeric reads while accepting lower re-
 858 call, which a conservative strategy appropriate for scenarios where false positives

859 are costly.

860 Feature importance analyses revealed that alignment disruptions, such as clip-
861 ping, and abrupt k-mer composition changes accounted for most predictive power.
862 In contrast, microhomology metrics and supplementary alignment descriptors con-
863 tributed minimally. These results indicate that features based on read alignment
864 and k-mer composition are sufficient to train classifiers for detecting mitochon-
865 drial PCR-induced chimera reads, without needing additional quality-score or
866 positional information in the conditions tested.

⁸⁶⁷ References

- ⁸⁶⁸ Anderson, S., Bankier, A., Barrell, B., Bruijn, M., Coulson, A., Drouin, J., ...
⁸⁶⁹ Young, I. (1981, 04). Sequence and organization of the human mitochondrial
⁸⁷⁰ genome. *Nature*, *290*, 457-465. doi: 10.1038/290457a0
- ⁸⁷¹ Arango, G., Garner, E., Pruden, A., Heath, L., Vikesland, P., & Zhang, L. (2018,
⁸⁷² 02). Deeparg: A deep learning approach for predicting antibiotic resistance
⁸⁷³ genes from metagenomic data. *Microbiome*, *6*. doi: 10.1186/s40168-018
⁸⁷⁴ -0401-z
- ⁸⁷⁵ Bentley, D. R., Balasubramanian, S., Swerdlow, H. P., Smith, G. P., Milton, J.,
⁸⁷⁶ Brown, C. G., ... Smith, A. J. (2008). Accurate whole human genome
⁸⁷⁷ sequencing using reversible terminator chemistry. *Nature*, *456*(7218), 53–
⁸⁷⁸ 59. doi: 10.1038/nature07517
- ⁸⁷⁹ Boore, J. L. (1999). Animal mitochondrial genomes. *Nucleic Acids Research*,
⁸⁸⁰ *27*(8), 1767–1780. doi: 10.1093/nar/27.8.1767
- ⁸⁸¹ Cameron, S. L. (2014). Insect mitochondrial genomics: Implications for evolution
⁸⁸² and phylogeny. *Annual Review of Entomology*, *59*, 95–117. doi: 10.1146/
⁸⁸³ annurev-ento-011613-162007
- ⁸⁸⁴ Dierckxsens, N., Mardulyn, P., & Smits, G. (2017). Novoplasty: de novo assembly
⁸⁸⁵ of organelle genomes from whole genome data. *Nucleic Acids Research*,

- 886 45(4), e18. doi: 10.1093/nar/gkw955
- 887 Edgar, R. C. (2016). Uchime2: improved chimera prediction for amplicon se-
888 quencing. *bioRxiv*. Retrieved from <https://api.semanticscholar.org/>
889 CorpusID:88955007
- 890 Edgar, R. C. (n.d.). *Uchime in practice*. Retrieved from https://www.drive5.com/usearch/manual7/uchime_practical.html
- 891 Edgar, R. C., Haas, B. J., Clemente, J. C., Quince, C., & Knight, R. (2011).
892 Uchime improves sensitivity and speed of chimera detection. *Bioinformatics*,
893 27(16), 2194–2200. doi: 10.1093/bioinformatics/btr381
- 894 Glenn, T. C. (2011). Field guide to next-generation dna sequencers. *Molecular
895 Ecology Resources*, 11(5), 759–769. doi: 10.1111/j.1755-0998.2011.03024.x
- 896 Gonzalez, J. M., Zimmermann, J., & Saiz-Jimenez, C. (2004, 09). Evalu-
897 ating putative chimeric sequences from pcr-amplified products. *Bioin-
898 formatics*, 21(3), 333-337. Retrieved from <https://doi.org/10.1093/bioinformatics/bti008>
899 doi: 10.1093/bioinformatics/bti008
- 900 Gray, M. W. (2012). Mitochondrial evolution. *Cold Spring Harbor perspectives
901 in biology*, 4. Retrieved from <https://doi.org/10.1101/cshperspect.a011403>
902 doi: 10.1101/cshperspect.a011403
- 903 Hahn, C., Bachmann, L., & Chevreux, B. (2013). Reconstructing mitochondrial
904 genomes directly from genomic next-generation sequencing reads—a baiting
905 and iterative mapping approach. *Nucleic Acids Research*, 41(13), e129. doi:
906 10.1093/nar/gkt371
- 907 Jin, J.-J., Yu, W.-B., Yang, J., Song, Y., dePamphilis, C. W., Yi, T.-S., & Li,
908 D.-Z. (2020). Getorganelle: a fast and versatile toolkit for accurate de
909 novo assembly of organelle genomes. *Genome Biology*, 21(1), 241. doi:
910 10.1186/s13059-020-02154-5
911

- 912 Judo, M. S. B., Wedel, W. R., & Wilson, B. H. (1998). Stimulation and sup-
913 pression of pcr-mediated recombination. *Nucleic Acids Research*, 26(7),
914 1819–1825. doi: 10.1093/nar/26.7.1819
- 915 Labrador, K., Agmata, A., Palermo, J. D., Ravago-Gotanco, R., & Pante, M. J.
916 (2021). Mitochondrial dna reveals genetically structured haplogroups of
917 bali sardinella (sardinella lemuru) in philippine waters. *Regional Studies in*
918 *Marine Science*, 41, 101588. doi: 10.1016/j.rsma.2020.101588
- 919 Li, H. (2018, 05). Minimap2: pairwise alignment for nucleotide sequences. *Bioin-*
920 *formatics*, 34(18), 3094-3100. Retrieved from <https://doi.org/10.1093/bioinformatics/bty191> doi: 10.1093/bioinformatics/bty191
- 922 Liang, Q., Bible, P. W., Liu, Y., Zou, B., & Wei, L. (2020, 02). Deepmi-
923 crobes: taxonomic classification for metagenomics with deep learning. *NAR*
924 *Genomics and Bioinformatics*, 2(1), lqaa009. Retrieved from <https://doi.org/10.1093/nargab/lqaa009> doi: 10.1093/nargab/lqaa009
- 926 Metzker, M. L. (2010). Sequencing technologies — the next generation. *Nature*
927 *Reviews Genetics*, 11(1), 31–46. doi: 10.1038/nrg2626
- 928 Mysara, M., Saeys, Y., Leys, N., Raes, J., & Monsieurs, P. (2015). Catch,
929 an ensemble classifier for chimera detection in 16s rrna sequencing stud-
930 ies. *Applied and Environmental Microbiology*, 81(5), 1573-1584. Retrieved
931 from <https://journals.asm.org/doi/abs/10.1128/aem.02896-14> doi:
932 10.1128/AEM.02896-14
- 933 Peccoud, J., Lequime, S., Moltini-Conclois, I., Giraud, I., Lambrechts, L., &
934 Gilbert, C. (2018, 04). A survey of virus recombination uncovers canon-
935 ical features of artificial chimeras generated during deep sequencing li-
936 brary preparation. *G3 Genes—Genomes—Genetics*, 8(4), 1129-1138. Re-
937 trieved from <https://doi.org/10.1534/g3.117.300468> doi: 10.1534/

- 938 g3.117.300468
- 939 Qin, Y., Wu, L., Zhang, Q., Wen, C., Nostrand, J. D. V., Ning, D., ... Zhou, J.
940 (2023). Effects of error, chimera, bias, and gc content on the accuracy of
941 amplicon sequencing. *mSystems*, 8(6), e01025-23. Retrieved from <https://journals.asm.org/doi/abs/10.1128/msystems.01025-23> doi: 10.1128/
942 msystems.01025-23
- 943
- 944 Qiu, X., Wu, L., Huang, H., McDonel, P. E., Palumbo, A. V., Tiedje, J. M., &
945 Zhou, J. (2001). Evaluation of pcr-generated chimeras, mutations, and het-
946 eroduplexes with 16s rrna gene-based cloning. *Applied and Environmental*
947 *Microbiology*, 67(2), 880–887. doi: 10.1128/AEM.67.2.880-887.2001
- 948 Ren, J., Song, K., Deng, C., Ahlgren, N., Fuhrman, J., Li, Y., ... Sun, F. (2020,
949 01). Identifying viruses from metagenomic data using deep learning. *Quan-*
950 *titative Biology*, 8. doi: 10.1007/s40484-019-0187-4
- 951 Rodriguez-Martin, B., Palumbo, E., Marco-Sola, S., Griebel, T., Ribeca, P.,
952 Alonso, G., ... Djebali, S. (2017, 01). Chimpipe: Accurate detection of
953 fusion genes and transcription-induced chimeras from rna-seq data. *BMC*
954 *Genomics*, 18. doi: 10.1186/s12864-016-3404-9
- 955 Rognes, T., Flouri, T., Nichols, B., Quince, C., & Mahé, F. (2016). Vsearch: a
956 versatile open source tool for metagenomics. *PeerJ*, 4, e2584. doi: 10.7717/
957 peerj.2584
- 958 Sedlazeck, F., Rescheneder, P., Smolka, M., Fang, H., Nattestad, M., von Haeseler,
959 A., & Schatz, M. (2018, 06). Accurate detection of complex structural
960 variations using single-molecule sequencing. *Nature Methods*, 15. doi: 10
961 .1038/s41592-018-0001-7
- 962 Sfeir, A., & Symington, L. S. (2015). Microhomology-mediated end joining: A
963 back-up survival mechanism or dedicated pathway? *Trends in Biochemical*

- 964 *Sciences*, 40(11), 701-714. Retrieved from <https://www.sciencedirect.com/science/article/pii/S0968000415001589> doi: <https://doi.org/10.1016/j.tibs.2015.08.006>
- 965
- 966
- 967 Vervier, K., Mahé, P., Tournoud, M., Veyrieras, J.-B., & Vert, J.-P. (2015,
968 11). Large-scale machine learning for metagenomics sequence classifica-
969 tion. *Bioinformatics*, 32(7), 1023-1032. Retrieved from <https://doi.org/10.1093/bioinformatics/btv683> doi: 10.1093/bioinformatics/btv683
- 970
- 971 Willette, D., Bognot, E., Mutia, M. T., & Santos, M. (2011). *Biology and ecology
972 of sardines in the philippines: A review* (Vol. 13; Tech. Rep. No. 1). NFRDI
973 Technical Paper Series. Retrieved from <https://nfrdi.da.gov.ph/tpjf/etc/Willette%20et%20al.%20Sardines%20Review.pdf>
- 974